Kinetics of the hydrodeoxygenation of cresol isomers over Ni$_2$P/SiO$_2$: Proposals of nature of deoxygenation active sites based on an experimental study

Vinicius O.O. Gonçalves [a], Priscilla M. de Souza [b], Victor Teixeira da Silva [b], Fabio B. Noronha [c,d], Frédéric Richard [a,*]

[a] Institut de Chimie des Milieux et Matériaux de Poitiers, UMR 7285 Université de Poitiers − CNRS, 4, rue Michel Brunet, BP633, 86022 Poitiers Cedex, France
[b] Universidade Federal do Rio de Janeiro, Chemical Engineering Program − COPPE, Caixa Postal 68502, CEP 21941-972, Rio de Janeiro, RJ, Brazil
[c] Catalysis Division, National Institute of Technology, Av. Venezuela 82, 20081-312, Rio de Janeiro, RJ 20081-312, Brazil
[d] Chemical Engineering Department, Military Institute of Engineering, Praça Gal. Tiburcio 80, 22290-270, Rio de Janeiro, RJ, Brazil

ARTICLE INFO

ABSTRACT

The hydrodeoxygenation of cresols (m-cresol, p-cresol and o-cresol) over Ni$_2$P/SiO$_2$ was carried out between 250 and 340 °C under high hydrogen pressure (between 1.6 and 3.2 MPa). XRD demonstrated that the desired Ni$_2$P phase was obtained at 450 °C using 4 MPa of H$_2$. The catalytic behavior of Ni$_2$P/SiO$_2$ for the transformation of cresols indicated that these compounds were deoxygenated by two different pathways, which involved different reactions such as hydrogenolysis, hydrogenation, dehydration and isomerization. Using these experimental conditions, i.e. under hydrogen pressure, the catalyst used exhibited a remarkable stability, at least during 20 h. An effect of the position of the methyl group in cresol isomers was highlighted, m-cresol being the most reactive whereas o-cresol the less reactive. In addition, an increase of temperature and hydrogen pressure allowed to ensure a high deoxygenation degree of phenolic reactants even at low level of conversion (less than 20%). The participation of different active sites and adsorption modes were proposed to explain the different products observed and their distribution.

© 2016 Elsevier B.V. All rights reserved.

1. Introduction

The use of lignocellulosic biomass as a renewable and sustainable source of energy is of growing importance due to the increasing attention on environmental concerns. Such raw materials could be transformed into chemicals and biofuels in a biorefinery [1–4]. The first step required is its depolymerization which can be carried out by several processes, including fast pyrolysis [3,5,6]. The bio-oil produced by fast pyrolysis has to be upgraded by hydrodeoxygenation (HDO) in order to reduce its oxygen content, leading to an oil with better physical and chemical properties such as higher heating values, lower viscosity, stability, pH values, and combustion properties compared to the crude bio-oil [7–11].

The type of catalyst play a key role on the HDO process. Conventional metal sulfides were extensively studied in such reactions due to their great importance in sulfur removal in oil processing [6,12–14]. Despite of their high activity in deoxygenation, sulfided catalysts have a drawback to process bio-oil since a sulfiding agent must be added to the reactant feed to keep the solid active and stable during the reaction, which could produce undesirable S-containing compounds in the final products [15–17]. Noble metal catalysts could be used as HDO catalyst due to their high activity in oxygen removal. [18–22]. Meanwhile, as they are highly expensive, their use for this purpose may be limited. Alternatively, the non-noble metal (e.g. Ni-based catalysts) are less costly than noble metal catalysts and also show acceptable deoxygenation performance [23–26]. However, Ni-based catalysts are known to promote secondary reactions like hydrogenolysis of C−C bond, methanation and decarbonylation, which results in a loss of carbon and a higher consumption of hydrogen. Transition metal phosphides have been proposed as catalysts for HDO of bio-oil [27–30]. The advantages of transition metal phosphides compared to other catalysts used in HDO are low cost when compared with noble metal catalysts, and the low selectivity for other reactions than deoxygenation with respect to non-noble metal catalysts [31–33].

Recent studies on deoxygenation of various phenolic model compounds such as phenol [34–36], guaiacol [37–41] and p-cresol [42,43] have shown that nickel phosphide based catalysts are effective catalysts in HDO. Zhao et al. [37] investigated the HDO of guaiacol under atmospheric pressure and 300 °C and found Ni_2P/SiO_2 to be more active to deoxygenation than a metallic phase (Pd/Al_2O_3) and a sulfide phase ($CoMo/Al_2O_3$). In addition, the same authors reported the HDO activity for different phosphide phases followed the order: $Ni_2P/SiO_2 > Co_2P/SiO_2 > Fe_2P/SiO_2 > WP/SiO_2 > MoP/SiO_2$. Indeed, nickel phosphide appeared as the most promising phosphide phase for HDO of various model oxygenated compounds [32,36,37,44,45], attributed to a higher d-electron density of the Ni_2P phase compared to other phosphide phases [45] but also to the presence of phosphorous that provides "ligand" (or electronic) and "ensemble" (or geometrical) effects on metal sites [39,45,46]. In fact, the ligand effect of P increases the electrophilicity of metal sites favoring the adsorption of oxygenated model compound, facilitating the C—O bond scission [31,45]. In general, catalytic behavior of different transition metal phosphides are interpreted in terms of the electron property of metal site, solid acidity or a combination of both [47]. Another interesting fact is the greater stability of phosphides compared to their parent metals. Indeed, during the HDO of anisole (1.5 MPa and 300 °C), Li et al. [45] assigned the higher stability of Ni_2P/SiO_2 compared to Ni/SiO_2 to the ligand effect given by P species, which would inhibit the combination of Ni with O and makes nickel phosphide catalyst more stable.

There are different reaction routes proposed for the HDO of phenol and alkylated phenols: direct deoxygenation (DDO) route; hydrogenation followed by dehydration (HYD) and tautomerization. The contribution of each route in the distribution of products is highly dependent on the nature of the active phase, as highlighted in recent reviews [7,10,14]. Over sulfided molybdenum-based catalysts, aromatics were favored over CoMoS phase, whereas the products formed by the HYD route (cycloalkenes and cycloalkanes) were predominated over both MoS_2 and NiMoS phases (under 4–7 MPa, 250–340 °C) [48–51]. Using nobel metal based-catalysts (i.e. Pd or Pt) under atmospheric pressure, aromatics appeared as the main deoxygenated products [20,21,52] meanwhile cycloalkanes were the main deoxygenated products under high pressure (10 MPa) [19]. In addition, oxophilic supports like ZrO_2 favored the selectivity to deoxygenated products due to the enhanced hydrogenation of the carbonyl function of the key intermediate suggested to be involved (phenolic tautomer) [20,21,52]. For the phosphide phases, the contribution of each deoxygenated route of phenolic compounds depended on the nature of the M_xP catalyst (Ni_2P, MoP, Fe_2P,...) and the experimental conditions [34–36,42,43,53]. Regarding the most active phosphide phase (i.e Ni_2P), it was reported that bulk Ni_2P yielded toluene as the main deoxygenated products from p-cresol [42], while methylcyclohexane appeared as the main deoxygenated product using the same reactant and under similar experimental conditions (325–350 °C, 4–4.4 MPa) [43]. Using phenol as model oxygenated molecule, the HYD route was also found to be predominant over different supported Ni_2P catalysts at 220 °C under 4 MPa [36]. Nevertheless, using the same oxygenated substrate, a modification of the selectivity of Ni_2P/SiO_2 was highlighted depending on the preparation method to obtain the phosphide phase [35]. These results show that the parameters which govern the selectivity of the Ni_2P phase are not yet completely known and hence require further investigation.

Therefore, the goal of this work was to investigate the catalytic properties of Ni_2P/SiO_2 catalyst for the hydrodeoxygenation of cresol isomers as model oxygenated compounds under high pressures of hydrogen (between 1.6 and 3.2 MPa) at temperatures between 250 and 340 °C. The different pathways involved during the transformations of such model molecules were carefully con-

sidered, in particular by using a kinetic model. The nature of active sites present on the nickel phosphide phase and reaction mechanisms were also discussed.

2. Experimental

2.1. Materials and chemicals

Silica was provided by Sigma-Aldrich. $Ni(NO_3)_2 \cdot 6H_2O$ (Merck), $(NH_4)_2HPO_4$ (Vetec) and HNO_3 (Merck) were used as precursors during the synthesis of the catalyst. The chemicals used for the reaction study (o-cresol, p-cresol, m-cresol, n-heptane and n-dodecane) were also purchased from Sigma-Aldrich. All chemicals were used without further purification. H_2 was provided by Air Liquide.

2.2. Catalyst synthesis

Prior to impregnation, silica was calcined under air flow at 800 °C for 5 h. The support was impregnated by nickel phosphide precursors using incipient wetness impregnation method (IWI), according to the procedure described by Yang et al. [31]. A solution containing the amounts of $(NH_4)_2 \cdot HPO_4$ and $Ni(NO_3)_2 \cdot 6H_2O$ required to obtain a Ni/P molar ratio of 2/1.6 and a nickel loading of 10 wt% was used. After impregnation, the solid sample was calcined under air at 500 °C for 3 h (2 °C min⁻¹).

2.3. Catalyst characterization

The chemical composition of the solid sample containing Ni_2P precursors was determined by inductively coupled plasma optical emission spectrometry (ICP-OES) using an SPECTRO ARCOS ICP-OES instrument. For this analysis, the sample was digested with concentrated nitric acid and hydrofluoric acid using microwave heating system.

N_2 adsorption−desorption isotherms were measured on a Micromeritics ASAP 2000 analyzer at −196 °C. Prior to N_2 adsorption, the solid samples containing oxide precursors were degassed overnight under secondary vacuum at 200 °C. The specific surface area (S_{BET} in $m^2 g^{-1}$) was calculated from the adsorption isotherm (P/P_0 between 0.05 and 0.20) using the Brunauer-Emmett-Teller (BET) method. The total pore volume was calculated from the adsorbed volume of nitrogen at P/P_0 equal to 0.99. The mesoporous volume was determined using the t-plot method. The average mesopore-size distribution was calculated from the adsorption isotherm branch using the Barret-Joyner-Halenda (BJH) method.

X-ray diffraction (XRD) pattern of the catalyst was collected between $2\theta = 20$ and 80° using a PAN-alytical EMPYREAN powder diffractometer using Cu-Kα monochromatized radiation source (Kα = 1.54059 Å). Phase identification was performed by comparison with the ICDS database reference files. The crystallite size (Dc) of Ni_2P particles was estimated by the Scherrer equation (Eq. (1)), as already reported [54]:

$$Dc = K\lambda/(\beta \cos\theta) \tag{1}$$

where K is the Scherrer constant (0.9), λ is the wavelength of the X-ray radiation (1.54059 Å), β is the width of the peak at half-maximum (FWHM) and θ is the Bragg angle. Prior to analysis, the nickel phosphide phase was obtained by performing the reduction of the catalyst in situ at 450 °C (5 °C min⁻¹) under 4 MPa as total pressure during 2 h using pure hydrogen (4.7 NL h⁻¹). After activation in situ, samples were cooled down under hydrogen until 25 °C and passivated at this temperature under atmospheric pressure for 3 h by a flow of 5 vol.% O_2 in He (80 mL min⁻¹).

In order to estimate the number of active sites and hence to calculate TOF values, CO chemisorption was performed at 30 °C. It was

assumed that CO-metal ratio was equal to 1, accordingly to Zhao et al. [37]. The solid containing oxide precursors (100 mg) was pretreated at 200 °C under helium (30 mL min^{-1}) for 30 min and cooled down to 50 °C. Then, the reduction was carried out in order to obtain the phosphide nickel phase under pure hydrogen (60 mL min^{-1}) at 700 °C (heating rate 5 °C min^{-1}), the final temperature was kept for 2 h. A DRX analysis performed after such treatment confirmed the formation of Ni$_2$P phase. The reactor was cooled down to the adsorption temperature (30 °C) under helium (30 mL min^{-1}). Successive pulses of pure CO (0.25 mL) were injected every 2 min. Results were collected by a gas phase chromatograph equipped with a TCD detector and a Porapak Q column (used to verify the absence of formation of CO$_2$ from CO) allowing the determination of the CO uptake value.

Temperature programmed reduction (H$_2$-TPR) was performed in a Micromeritics AutoChem 2910. Prior to reduction, the sample (100 mg) was pretreated under He flow (20 mL min^{-1}) at 200 °C (heating rate of 10 °C min^{-1}) for 30 min. Then the catalyst was cooled down to 50 °C. The reduction measurements started at this temperature using 10% H$_2$ in Ar (20 mL min^{-1}). The temperature was progressively increased until 1000 °C (heating rate 5 °C min^{-1}) and held for 90 min. The hydrogen consumption was estimated using a TCD detector.

In order to determine the acidity of the phosphide phase, NH$_3$-TPD was carried out using 150 mg of solid samples: the bare SiO$_2$ and the nickel phosphide catalyst obtained after the activation procedure (450 °C under 4 MPa of H$_2$) and then passivated (details in the XRD analysis description). The samples were pretreated with He (30 mL min^{-1}) at 200 °C for 30 min, and cooled down to 100 °C. The solids were then exposed to a flow containing 5% NH$_3$ in He (30 mL min^{-1}) for 30 min. The physisorbed ammonia was purged with He (30 mL min^{-1}) for 1 h. Desorption was measured under a heating of 5 °C min^{-1} under He to 600 °C with a plateau at this temperature for 1 h. The measurements of desorbed NH$_3$ quantities were continuously monitored by a TCD detector.

The nickel phosphide phase was obtained by performing the reduction of the catalyst in situ at. After activation in situ, samples were cooled down under hydrogen until 25 °C and passivated at this temperature under atmospheric pressure for 3 h by a flow of 5 vol.% O$_2$ in He (80 mL min^{-1}).

2.4. Catalytic experiments

The HDO of cresol (o-, m- and p-cresol) was performed in a fixed-bed reactor (length: 40 cm; inner diameter: 1.26 cm) at 340 °C under 4 MPa. Prior to reaction, the catalyst (pelleted, crushed and sieved to 250–315 μm) were reduced in-situ at 450 °C (5 °C min^{-1}) under 4 MPa as total pressure for 2 h using pure hydrogen (4.7 NL h^{-1}). The reactor was continuously fed by a liquid model feed prepared to obtain 53 kPa of the oxygenated reactant and 31 kPa of n-heptane used as an internal standard diluted with n-dodecane. The hydrogen to oxygenate molar ratio was kept as 486 NL L^{-1}.

Experiments were performed during 20 h on stream (TOS). Different conversion levels (conversions lower than 25%) were obtained varying the space time (τ in g h mol^{-1}, defined in Eq. (2)) every 5 h on stream. For a single experiment, space times were varied by changing the reactant flow.

$$\tau = \frac{w}{F_{CRE}} \tag{2}$$

where w is the weight of catalyst and F$_{cresol}$ the molar flow rate of the oxygenated model compound fed into the reactor. For all experiments, the mass balances were always between 95 and 100%, in accordance with study carried out with the same type of reactant [42]. The absence of internal mass-transfer effect was confirmed

by the calculation of the Weisz-Prater criteria (see supplementary information, Table S1) [44,55,56]. In addition, it was verified the absence of external diffusion. Indeed, the conversion of cresols remained constant when a variation of the molar flow rate at the reactor entrance was compensated by a proportional variation of the catalyst weight. Moreover, it was previously verified that n-heptane and n-dodecane were unreactive in presence of Ni$_2$P/SiO$_2$. The reproducibility of a set of experiment is given in supplementary information (Table S2), which shows that the same data was obtained from different experiments using the same experimental conditions.

The reaction products were periodically collected from the condenser (Minichiller-Huber cryostat) and analyzed by a Varian 430 chromatograph equipped with a DB1 capillary column (length: 30 m, inside diameter: 0.320 mm, film thickness: 5 μm) and a flame ionization detector (FID). All products were identified by using a 1200 TQ mass spectrometer coupled with a Varian 3800 chromatograph and by co-injection of commercial compounds.

The reactant conversion (X$_{cresol}$ in%) was calculated according to Eq. (3):

$$X_{CRE} = \frac{C_{CRE,0} - C_{CRE}}{C_{CRE,0}}.100 \tag{3}$$

C$_{CRE,0}$ being the initial molar concentration of the cresol isomer and C$_{CRE}$ as the molar concentration of the corresponding reactant in the liquid sample collected at the studied space time τ.

The selectivity and the yield of a product i (S$_i$ in mol%) are given by Eqs. (4) and (5), respectively:

$$S_i = \frac{C_i}{C_{CRE,0} - C_{CRE}}.100 \tag{4}$$

$$Y_i = S_i.X_{CRE}/100 \tag{5}$$

where C$_i$ represents the molar concentration of a product "i" in the liquid sample analyzed.

Assuming the reaction as pseudo-first order, the total apparent rate constant (k$_{TOT}$, in mmol h^{-1} g^{-1}) and the turnover frequency (TOF, in h^{-1}) values can be calculated using Eqs. (6) and (7), respectively:

$$k_{TOT} = {}^1/\tau.\ln(1 - X_{CRE}) \tag{6}$$

$$TOF = k_{TOT}/M \tag{7}$$

where M is the CO uptake (in mmol g^{-1}) obtained from chemisorption measurement.

2.5. Elemental analysis of spent catalysts

Chemical analysis of carbon and hydrogen were carried out after reaction test by using an elemental analyzer (NA2100 analyzer, CE instruments). The spent catalysts were characterized without chemical treatment.

3. Results and discussion

3.1. Catalyst characterization

From ICP analysis, the catalyst after the reduction procedure contained 9.0 wt% of nickel which corresponds to 11.3 wt% of Ni$_2$P. Fig. 1 shows the XRD pattern of the catalyst after the reduction at 450 °C under 4 MPa of hydrogen. A broad peak was observed at 2θ ≈ 22° characteristic of the amorphous silica. All characteristic diffraction peaks of the Ni$_2$P phase were observed (ICDS 98-064-6102) indicating that the reduction procedure allowed to obtain the desired nickel phosphide phase (Ni$_2$P). Interestingly, using the same Ni/P ratio, it was observed in the literature that Ni$_{12}$P$_5$ was
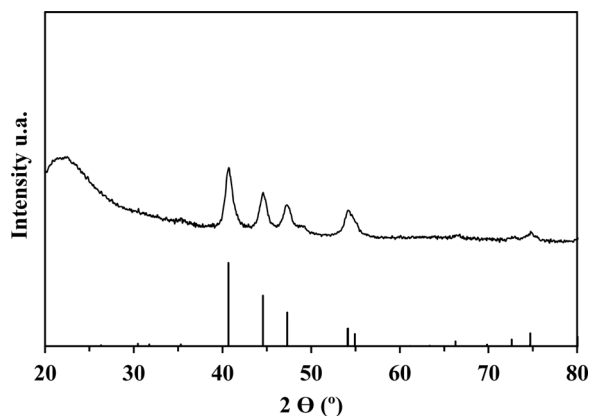
Fig. 1. XRD diffraction pattern for Ni_2P/SiO_2 obtained after reduction procedure carried out at 450 °C under 4 MPa of H_2 (ICDS 98-064-6102 file appears at the bottom of the figure).
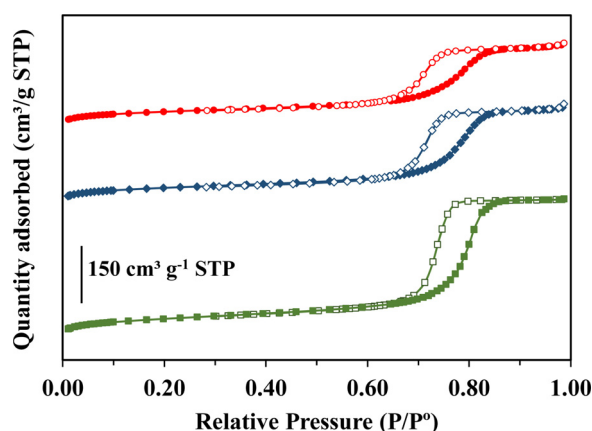

Fig. 2. Nitrogen adsorption-desorption isotherms of bare silica (■), silica containing oxide precursors (◆), silica containing Ni_2P phase after reduction at 450 °C and 4 MPa of H_2 (●). Full symbols for adsorption and empty symbols for desorption.

favored at reduction temperatures lower than 550 °C when the activation procedure was carried out under atmospheric pressure [57]. It should be mentioned that $Ni_{12}P_5$ phase is known to be less active for HDO than Ni_2P [37]. Consequently, the activation procedure carried out under 4 MPa of H_2 allowed to decrease significantly the reduction temperature required to achieve the formation of Ni_2P phase, which usually ranged between 600 and 700 °C, as reported in the literature [29]. In addition, the average crystallite size of Ni_2P calculated by the Scherrer equation was about 12 nm, close to values already reported using a similar loading (7.91%) of the same phosphide phase [58].

Fig. 2 displays the adsorption-desorption isotherms of different materials: the bare silica, the silica containing oxide precursors ($Ni_xP_yO_z$) and the silica containing Ni_2P phase obtained after reduction under 4 MPa of H_2 and 450 °C. According to the IUPAC classification, all isotherms were typical of mesoporous materials (type IV), and exhibited H_2 type hysteresis due to the presence of "ink-bottle" pore [59]. As shown in Table 1, the impregnation of oxides on silica led to a decrease in the specific surface area (15%) and pore volume (39%). This trend can be mainly explained by introduction of both precursors leading to a partial blockage of the porous system. The reduction step required to obtain the Ni_2P phase had practically no effect on the specific surface area but led to a further decrease in the pore volume (15%) and a small reduction of the pore diameter of silica. These results seem to indicate that the formation of the nickel phosphide phase impact only slightly on the porosity of the support used.
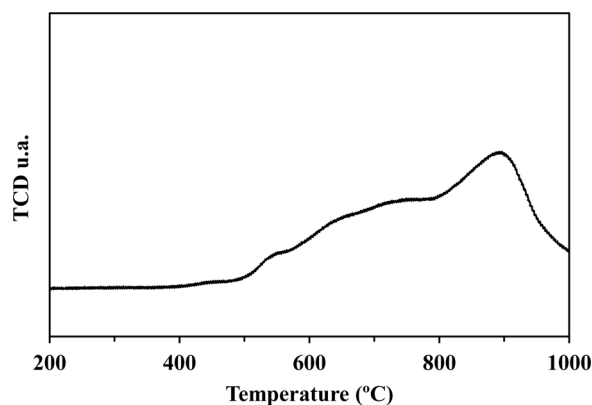

Fig. 3. H_2-TPR profile of Ni_2P/SiO_2.

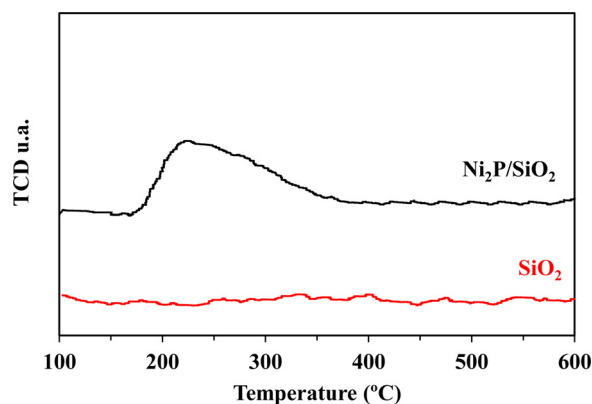**Fig. 4.** NH_3-TPD profile of Ni_2P/SiO_2 and bare SiO_2.

The CO uptake measurement is often used to provide an estimation of the number of active sites presents on nickel phosphide phase [29]. Using FT-IR analysis, it was proposed that CO was bounded to the Ni sites on Ni_2P [60], such sites were probably involved for adsorption of cresol isomers, and will be discussed in the next part of the present manuscript. The value measured in our case (M = 33 μmol g^{-1}) was close to values reported for similar loading of Ni_2P phase [61,62]. Based on experiments Infrared analysis using CO as a probe molecule, it was proposed that this molecule was bound on the Ni sites on nickel phosphide phase, as

Fig. 3 shows the TPR profile of the oxyphosphate precursors ($Ni_xP_yO_z$) which reveals several peaks in the range of 400–1000 °C. Since this sample was prepared from the mixture of nickel and phosphorus precursors, nickel is likely to be in the form of phosphate ($Ni_xP_yO_z$), as proposed by several authors [40,58]. This may explains why the reduction occurred at higher temperature than observed for nickel oxide samples, usually at lower temperatures than 550 °C [19,26]. As expected, no consumption of H_2 was observed during the analysis of bare SiO_2. The value of H_2 uptake obtained for Ni_2P/SiO_2 was equal to 4.10 mmol g^{-1}, this value is about 16% higher than the theoretical value (equal to 3.45 mmol g^{-1}) calculated to form Ni_2P from the quantity of NiO present on silica (9.0% of Ni). Thus, the excess of hydrogen consumed (about 0.65 mmol g^{-1}) could correspond to the reduction of P-O bond leading to the formation of PH_3, centred at 800 °C. In the same way, Oyama and co-workers [63], demonstrated that some phosphorus present in the support can be release in the TPR step as PH_3.

The acid properties of the Ni_2P/SiO_2 catalyst were determined using a NH_3 thermodesorption experiment (NH_3-TPD). Fig. 4 shows a broad peak centred at around 235 °C indicating that its acidity

Table 1
Textural properties of pure silica (SiO_2), supported nickel phosphide precursors ($Ni_xP_yO_z/SiO_2$) and supported nickel phosphide (Ni_2P/SiO_2) solids determined by adsorption-desorption of nitrogen.

	S_{BET} ($m^2 g^{-1}$)	Pore volume[a] ($cm^3 g^{-1}$)	Mesoporous volume[b] ($cm^3 g^{-1}$)	Average pore diameter[c] (nm)
SiO_2	208	0.57	0.54	9
$(NiO + P_2O_5)/SiO_2$	176	0.40	0.33	8
Ni_2P/SiO_2	172	0.34	0.27	7

[a] calculated at P/P_0 equal to 0.98.
[b] deduced from the t-plot method.
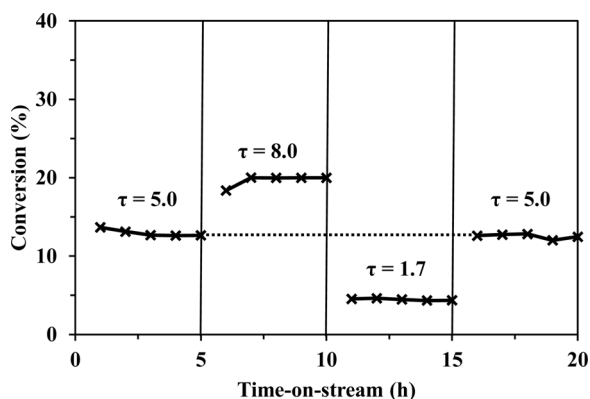[c] deduced from the BJH method using the adsorption branch.

Fig. 5. Conversion of m-cresol under 4 MPa and 340 °C over Ni_2P/SiO_2 as function of time-on-stream (τ in g h mol^{-1}).

Table 2
Chemical composition in carbon and hydrogen of spent catalysts, obtained after 20 h on stream at 340 °C under 4 MPa as total pressure.

Model molecule	C (wt%)	H (wt%)	C/H
o-cresol	6.4	0.6	11
m-cresol	6.7	0.6	11
p-cresol	6.0	0.5	12

($123 \mu mol g^{-1}$) is quite weak and only attributed to the phosphide phase since bare SiO_2 did not exhibit any NH_3 adsorption. Similar profile was already reported by Wu et al. for the same type of catalyst [40]. In addition, using pyridine as a probe molecule, it was proposed that nickel phosphide phase exhibited both Lewis acid sites (attributed to $Ni^{\delta+}$ species) and Brønsted acid sites (ascribed to PO—H groups) [54,55,64].

3.2. Catalytic properties of Ni_2P/SiO_2 during HDO of cresol isomers

The hydrodeoxygenation of cresol isomers was studied at 340 °C under 4 MPa of total pressure over Ni_2P/SiO_2 during 20 h time on stream. As shown in Fig. 5, the conversions of m-cresol obtained at the beginning and after 20 h on stream at the same τ (5.0 g h mol^{-1}) were quite similar, which indicates that Ni_2P/SiO_2 was quite stable under these experimental conditions, in spite of amount of carbon measured on this catalyst after reaction (between 6 and 7 wt.%, Table 2). As no deactivation was observed, the amount of carbon deposited can be attributed to the presence of adsorbed oxygenated reactants rather than heavy molecules explaining why the catalyst exhibited a good stability. Indeed, the C/H ratios determined on the spent catalysts (close to 11) were of the same order of magnitude than the corresponding ratio calculated for cresol isomers (C_7H_8O, which C/H is equal to 10.5). Therefore, the use of a high pressure of hydrogen (3.2 MPa) prevented the deactivation of the nickel phosphide phase. On the contrary, a strong deactivation rate was observed during HDO of guaiacol carried out under atmospheric pressure over Ni_2P/SiO_2 [38,40]. This deactivation was

mainly attributed to coke accumulation. Li et al. [45] also reported a significant deactivation of Ni_2P/SiO_2 studying the deoxygenation of anisole at 300 °C under mild pressure (1.5 MPa). This result was assigned to a modification of the phosphide phase leading to the formation of inactive phosphate species. Such modification does not occur in our case, confirming the beneficial role of a high pressure of H_2 on the stability of nickel phosphide phase. These results are in accordance with the positive effect of pressure in the pyrolysis bio-oil upgrading steps proposed by Koike et al. [65].
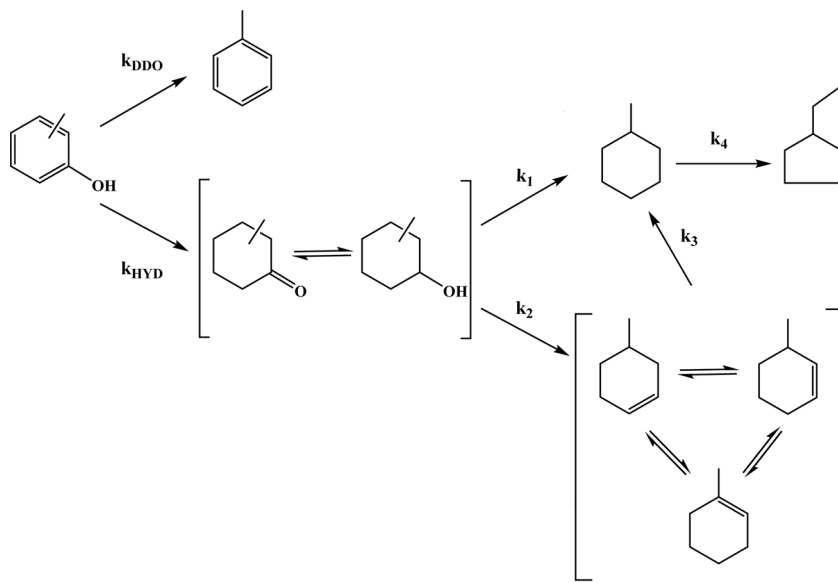
Various products were detected during the transformation of cresols under 4 MPa at 340 °C: aromatic (toluene), oxygenates (methylcyclohexanol and methylcyclohexanone isomers), alkenes (1-, 3- and 4-methylcyclohexene) and naphthenic (methylcyclohexane and ethylcyclopentane) compounds. Their quantities varied depending on the reactant, the operating conditions and the conversion (Table 3 and Fig. 5). Regardless of the cresol isomer, the selectivity into deoxygenated products was higher than 79% and methylcyclohexane was the main deoxygenated product at about 20% of conversion, its selectivity varying from 56 to 65 mol% (Table 3). Fig. 6 shows that the yield into toluene increased linearly with the conversion of cresol isomers indicating that toluene was unreactive under these experimental conditions. This is in line with the fact that anisole and phenol were converted into either benzene or cyclohexane, the former being favored under atmospheric pressure, whereas the latter was favored at higher pressure (0.8 MPa) [39]. Thus, in this study, the hydrogenation of benzene was never observed. In addition, toluene was favored when m-cresol was used as reactant, its selectivity being close to 20 mol% while only half of this amount was obtained from the other two isomers (Table 3).

Oxygenates and alkenes appeared as intermediates since their yield reached a maximum and then decreased (Fig. 6). It can be pointed out that the amount of oxygenates were highly dependent on the reactant. As indicated in Table 3, o-cresol led to the highest quantity of oxygenates and m-cresol the lowest, 21.0 and 1.6 mol%, respectively. These results indicate an important effect of the position of the methyl group on the reactivity of these compounds. Indeed, the selectivity into ketone varied according to the followed order: o-cresol > p-cresol > m-cresol. This result demonstrates that the methyl group in ortho position limit the hydrogenation of the ketone function. The selectivity into methylcyclohexene isomers were similar for all cresols, ranging 10–15 mol%. Interestingly, 1-methylcyclohexene was always the main alkene isomer. Based on thermodynamics, the percentage of this isomer is expected to be equal to 65 mol% [66], and very close to the experimental values reported in Table 3 (between 63 and 65 mol%). This indicates that the methylcyclohexene isomers were observed in thermodynamic equilibrium. From m-cresol and p-cresol, 1-methylcyclohexene was not expected. Its formation can be explained by the double-bond migration due to the acidity of the phosphide phase. Moreover, ethylcyclopentane was also detected in trace amounts. Its appearance is also linked to the acidic properties of Ni_2P/SiO_2, resulting in an isomerization of methylcyclohexane.

From our experimental results, and accordingly to the literature data obtained from the HDO of cresol isomers on Ni_2P phase [42,43],

Table 3
Transformation of cresol isomers at 340 °C under 4 MPa of total pressure over Ni_2P/SiO_2 (conversion close to 20%).

Model molecule	τ (g h mol^{-1})	Conversion (%)	Selectivity (mol%)						1-MCHe/MCHes
			Tol	MCHnone	MCHols	MCHes	MCH	ECP	
o-cresol	11.0	18.7	8.2	13.6	7.4	14.4	55.7	0.7	65
m-cresol	8.0	20.2	20.6	1.6	0.0	13.8	62.9	1.1	65
p-cresol	9.0	19.4	10.2	4.1	7.1	10.0	64.8	3.8	63

Scheme 1. Reaction scheme for the transformation of cresol isomers over Ni_2P/SiO_2.

it can be considered that the formation of those products proceeded via two parallel reaction pathways as described in Scheme 1. Toluene was produced by direct cleavage of C—O bond (DDO pathway) whereas the other products were obtained by hydrogenation, hydrogenolysis and dehydration reactions (HYD pathway) leading to naphthenic compounds (methylcyclohexane and ethylcyclopentane) as final products. It is noteworthy to mention that methylcyclohexane can be either produced by hydrogenolysis of methylcyclohexanol (estimated by k_1) or by hydrogenation of methylcyclohexenes isomers, which can be obtained by dehydration the alcohol (estimated by k_2).

In order to obtain more information about the transformation of all cresol isomers, a kinetic analysis was employed using an adequate power law model, similar to the equation already used to model the HDO of cresols over sulfide catalysts [51]. In this case, a proper equation can be written:

$$-r_{Tot} = \frac{dC_{CRE}}{d\tau} = -kC_{CRE}^{\alpha}P_{H_2}^{\beta} \tag{8}$$

where r_{Tot} is the total rate of the transformation of cresols, k is the reaction rate constant, C_{CRE} the molar concentration of a given cresol, P_{H_2} the partial pressure of hydrogen, τ the space time defined previously, α the reaction order in the cresol isomer, and β the reaction order in H_2.

As hydrogen was used in a large excess compared to cresols, the hydrogen partial pressure was assumed to be constant. In addition, according to Fig. 7, the plot of $-\ln(1-X_{CRE})$ as function of space times displays a pseudo-first order behavior for the three cresol isomers, as proposed to describe kinetics from the HDO of p-cresol [42]. Consequently, Eq. (8) can be simplified as follows:

$$-r_{Tot} = \frac{dC_{CRE}}{d\tau} = -k_{Tot}C_{CRE} \tag{9}$$

where k_{Tot} is the global apparent constant.

The total kinetic apparent rate constants (k_{Tot}) measured for the three cresol isomers are given in Table 4 and followed the order m-cresol > p-cresol > o-cresol, indicating that the reactivity of cresols was dependent on the position of the methyl group. The same reactivity scale was reported over sulfide catalysts under the same experimental conditions (340 °C, 4 MPa) [51]. In addition, it was observed that the total rate constant using o-cresol as reactant (equal to 18.8 mmol g^{-1} h^{-1}) was close to the one determined for a sulfided CoMo/Al$_2$O$_3$ catalyst (25 mmol g^{-1} h^{-1}, value reported in [51]). Nevertheless, this sulfide phase was about twice as active as the phosphide phase for the HDO of m-cresol. As expected, the TOF values followed the same order as k_{Tot}, in the range of 570 and 858 h^{-1}. These values were considerably higher than those reported in the literature for several phenolic compounds at 300 °C under mild and atmospheric pressures [37,40,45]. As an example, using guaiacol as model reactant, Wu et al. found that the TOF value was 220 h^{-1} under atmospheric conditions using Ni$_2$P/SiO$_2$ as catalyst [40]. Due to the mesoporosity of the support (as shown in Table 1), it can be assumed that all active sites were accessible to the cresol isomers.

The kinetic modeling based on the proposed reaction network can be performed using an integral method. In this case, following Scheme 1, several differential equations related to the transformation of cresols can be written. For a shake of simplicity, the concentrations of oxygenated compounds have been put together and named C_{oxy}.

$$\frac{dC_{CRE}}{d\tau} = -(k_{DDO} + k_{HYD})C_{CRE} \tag{10}$$

$$\frac{dC_{Tol}}{d\tau} = k_{DDO}C_{CRE} \tag{11}$$

$$\frac{dC_{Oxy}}{d\tau} = k_{HYD}C_{CRE} - k_1 C_{Oxy} - k_2 P_{Oxy} \tag{12}$$

Table 4
Individual apparent rate constants determined during the transformation of cresol isomers at 340 °C under 4 MPa of total pressure over Ni_2P/SiO_2 (standard deviation of rate constants close to 5%).

Model molecule	Rate constants (in mmol h^{-1} g^{-1})							TOF (h^{-1})
	k_{Tot}	k_{DDO}	k_{HYD}	k_1	k_2	k_3	k_4	
o-cresol	18.8 ± 0.9	1.5 ± 0.1	17.3 ± 0.9	345 ± 17	31 ± 2	482 ± 24	23 ± 1	570 ± 29
m-cresol	28.3 ± 1.4	5.8 ± 0.3	22.5 ± 1.1	2254 ± 113	166 ± 8	552 ± 30	39 ± 3	858 ± 43
p-cresol	24.0 ± 1.2	2.5 ± 0.1	21.5 ± 1.1	605 ± 30	318 ± 16	599 ± 28	54 ± 2	727 ± 36

Fig. 7. Pseudo-first order plots obtained from the HDO of cresol isomers over Ni_2P/SiO_2 under 4 MPa at 340 °C; o-cresol (▲), m-cresol (■) and p-cresol (●).
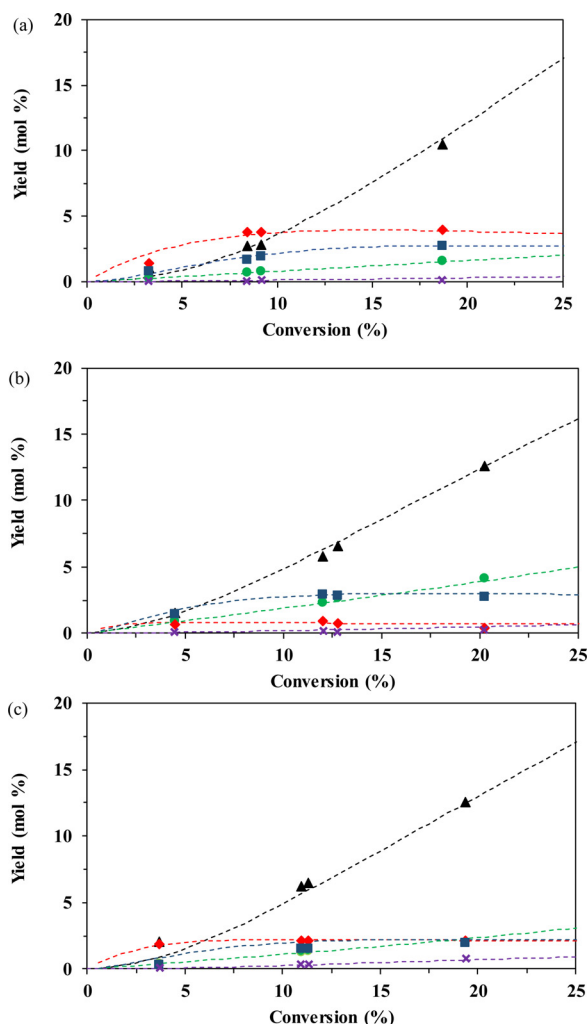
Fig. 6. Experimental (symbols) and calculated (lines) yields into products from the transformation of o-cresol (a), m-cresol (b) and p-cresol (c) over Ni_2P/SiO_2 at 4 MPa and 340 °C; methylcyclohexane (▲) methylcyclohexenes (■), oxygenates (◆), toluene (●), ethylcyclopentane (✕).

$$\frac{dC_{MCHes}}{d\tau} = k_2 C_{Oxy} - k_3 C_{MCHes} \qquad (13)$$

$$\frac{dC_{MCH}}{d\tau} = k_1 C_{Oxy} + k_3 C_{MCHes} - k_4 C_{MCH} \qquad (14)$$

$$\frac{dC_{ECP}}{d\tau} = k_4 C_{MCH} \qquad (15)$$

where k_{DDO}, k_{HYD}, k_1, k_2, k_3, k_4 are the intrinsic rate constants involved in the transformation of cresol isomers. C_{Tol}, C_{Oxy}, C_{MCHes}, C_{MCH} and C_{ECP} are the molar concentration of toluene, oxygenates, methylcyclohexenes, methylcyclohexane and ethylcyclopentane, respectively.

The system of equations above (Eqs. (10)–(15)) was solved applying Runge–Kutta 4th order numerical integration algorithm.
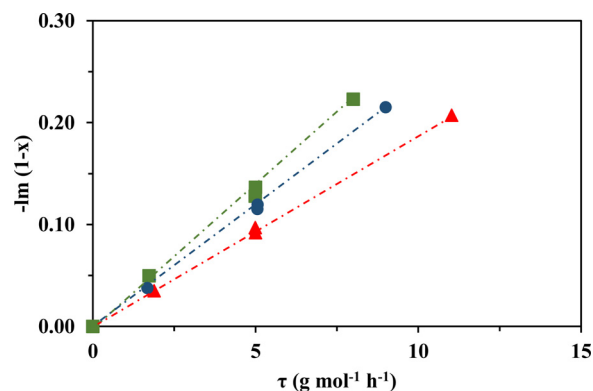
Data fitting was performed by minimizing the residual sum of squares (RSS, Eq. (16)) between the molar concentration of each product obtained experimentally and the calculated values. The results of modeling for Ni_2P/SiO_2 are presented in Fig. 6, which shows the yield of each product as function of conversion.

$$RSS = \sum \left(C_{i,exp} - C_{i,cal} \right)^2 \qquad (16)$$

where $C_{i,exp}$ and $C_{i,cal}$ are the experimental and calculated partial pressure of component

The kinetic rates obtained from data fitting, presented in Table 4, showed that the reaction proceeds mainly toward the HYD route (k_{HYD}/k_{DDO} between 4 and 12, depending on the cresol isomer). According to the data, it appears that the influence of the position of the methyl group is more important on the DDO route than on the HYD route. Indeed, k_{DDO} measured from m-cresol was more than twice as high as this rate constant for p-cresol, whereas the values of k_{HYD} for both reactants were very close. In addition, o-cresol was the less reactive isomer regardless of the deoxygenation route, which is likely due to a steric hindrance attributed to the methyl group in the vicinity of the OH group. Such steric effect was already described for the HDO reaction of cresols but only over CoMoS catalysts [51,67].

For all reactants, the k_1 values were always higher than k_2, showing that alcohols were mainly deoxygenated by hydrogenolysis of the C—O bond to methylcyclohexane (estimated by k_1) rather than by dehydration yielding methylcyclohexenes (estimated by k_2). This result can be explained by a weak acidity of the phosphide phase leading to a low rate of the alcohol dehydration. In addition, the order of reactivity of alcohol intermediates was dependent on the type of reaction involved. Thus, the sequence of reactivity followed 3-MCHols > 4-MCHols > 2-MCHols for hydrogenolysis (k_1 values), while the sequence was 4-MCHols > 3-MCHols > 2-MCHols for dehydration (k_2 values). Moreover, the sequence of reactivity determined previously for C—O hydrogenolysis of alcohols isomers (estimated by k_1 values) was the same than the one determined for the direct C—O bond scission of cresols (estimated by k_{DDO}). These results seem to indicate that the effect of the position of the methyl group was the same for both C—O bond scissions, suggesting that
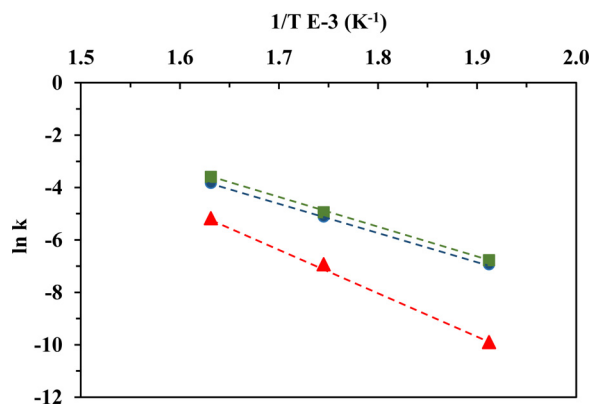
Fig. 8. Influence of the temperature on the kinetic rate constants (k_{Tot}: ■ ; k_{DDO}: ▲ and k_{HYD}: ●) determined during the transformation of m-cresol over Ni_2P/SiO_2. Ln k as function of 1/T.

Fig. 9. Influence of the pressure of H_2 on the kinetic rate constants (k_{Tot}: ■ ; k_{DDO}: ▲ and k_{HYD}: ●) determined during the transformation of m-cresol over Ni_2P/SiO_2. Ln k as function of ln (P_{H2}).

active sites involved in both reactions could be similar in nature. In addition, k_1 values were much higher than k_{DDO} values since the C—O bond strength of a phenolic compound is about 80 kJ mol^{-1} greater compared to an aliphatic alcohol [12].

As for the dehydration rate of methylcyclohexanols (k_2), the isomerization of methylcyclohexane into ethylcyclopentane (measured by k_4) is related to the acidic properties of Ni_2P/SiO_2. The k_4 values should not be very dependent on the cresol isomer used. Moreover, as expected, the k_3 rate constants were practically not dependent on the starting cresol, since these values estimated the hydrogenation rate of methylcyclohexenes which were obtained in thermodynamic quantities. However, the mixture of methylcyclohexenes was found in thermodynamic equilibriums which might explain why these values were close for all cresol isomers (Table 4).

The influence of temperature was also investigated between 250 °C and 340 °C for the conversion of m-cresol under 4 MPa as total pressure (Table 5). As expected, an increase of the temperature led to an increase in the activity of Ni_2P/SiO_2 as shown in Fig. 8. The apparent activation energy (E_a) can be calculated by the Arrhenius equation (Eq. (17)):

$$\ln k_{Tot} = \ln A - \frac{E_a}{RT} \qquad (17)$$

where k_{Tot} is the total rate constant at a given reaction temperature, A corresponds to the frequency factor, E_a is the apparent activation energy, R is the universal gas constant, and T is the reaction temperature (K). In order to calculate the apparent activation energy of both deoxygenation routes, $E_{a,HYD}$ and $E_{a,DDO}$, k_{Tot} was replaced by k_{HYD} and k_{DDO} in Eq. (17), respectively. The calculated activation energy for hydrodeoxygenation of m-cresol was 95 kJ mol^{-1}. Regarding the different pathways, the E_a of the HYD pathway was close to the overall reaction (90 kJ mol^{-1}) since it was the main pathway for the transformation of m-cresol. The E_a of the DDO route was higher, close to 138 kJ mol^{-1}. Consequently, an increase of the temperature favors the DDO route over the HYD route, explaining the decrease of the k_{HYD}/k_{DDO} ratio with increasing temperature. Thus, the k_{HYD}/k_{DDO} ratio was equal to 10 at 250 °C and close to 4 at 340 °C. These results seem to confirm that active sites involved in the direct C—O bond scission (DDO route) and in hydrogenation of the aromatic ring (the initial step of the HYD route) could be different in nature. This particular point will be further discussed.

Increasing the temperature decreased the selectivity to 3-MCHnone and 3-MCHols indicating a beneficial effect of the temperature on the deoxygenation degree of m-cresol (see entries 1–3 in Table 5). As a result, the oxygenated products accounted for approximately 22 mol% of all products at 250 °C and only 5 mol% at 340 °C. The increase of temperature favored the pro-
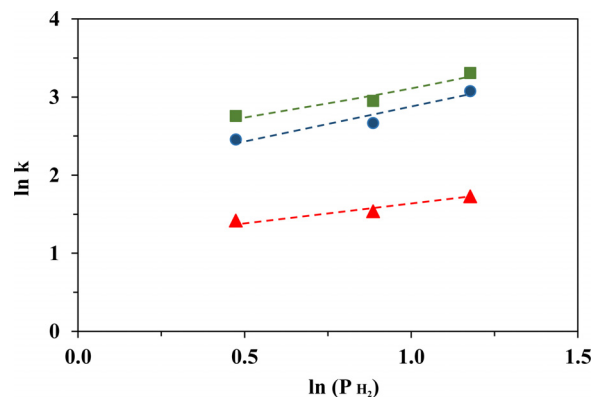
duction of toluene; its selectivity increased by almost four-fold between 250 and 340 °C. This increase can be explained both by kinetics (as shown in Fig. 8), but also by thermodynamics, aromatic being favored compared to naphthenic compounds at higher temperatures [14]. The increase of temperature increased the selectivity to methylcyclohexane whereas the formation of methylcyclohexene decreased. Indeed, the alkane/alkenes ratio was equal to 0.9 at 250 °C and it rose to 2.4 at 340 °C. However, the total amount of methylcyclohexane and methylcyclohexene remained constant for all reaction temperatures. These results suggest that an increase of the temperature favors both the hydrogenolysis of methylcyclohexanols and the hydrogenation of methylcyclohexenes. In addition, as shown in Table 5, the slight decrease of the 1-methylcyclohexene/methylcyclohexenes ratio with temperature can be attributed to thermodynamics [66].

The effect of H_2 pressure was also evaluated for the HDO of m-cresol over Ni_2P/SiO_2, the temperature being kept constant at 340 °C. Fig. 9 shows that an increase of the partial pressure of H_2 resulted in a significant increase of k_{Tot} indicating a benefit for the catalytic activity of Ni_2P/SiO_2. It is observed that the k_{Tot} value practically doubled when partial pressure of hydrogen increased from 1.6 MPa to 3.2 MPa, the apparent global kinetic order of H_2 being close to 1. It can also be noted that the HYD pathway was promoted by increasing hydrogen pressure, whereas the DDO pathway was only slightly improved. The kinetic partial order of H_2 was dependent on the deoxygenation route: 0.8 for HYD route and 0.5 for DDO route. Therefore, the k_{HYD}/k_{DDO} ratio increased with the pressure of H_2, being 2.8 under 1.6 MPa and close to 4 under 3.2 MPa. These results clearly indicated that an increase in the pressure of H_2 was beneficial for the HDO of phenolic compounds, in agreement with results reported by Moon et al. [39]. Nevertheless, the effect of pressure was dependent on the deoxygenation route involved. The positive effect of hydrogen was higher on the HYD route than on the DDO route. This fact can be easily explained since the HYD route needs a higher quantity of hydrogen to be performed than the DDO route.

The product distribution from the HDO of m-cresol at different H_2 pressure obtained at similar conversion levels are given in Table 5 (entries 3–5). It is important to mention that an increase of partial pressure of H_2 decreased the selectivity into oxygenated products, hence favoring the deoxygenation degree of m-cresol. However, the selectivity to toluene decreased from 26.2 mol% to 20.7 mol% when the partial pressure of H_2 increased from 1.6 MPa to 3.2 MPa. This trend can also be explained by both thermodynamics and kinetics. Indeed, it is known that the thermodynamic equilibrium between cyclohexane and benzene can shift in favor of alkane with an increase of the pressure of H_2 [39]. From kinetics

Table 5
Effect of temperature and partial pressure of H_2 on the HDO of m-cresol over Ni_2P/SiO_2 (conversion close to 10%).
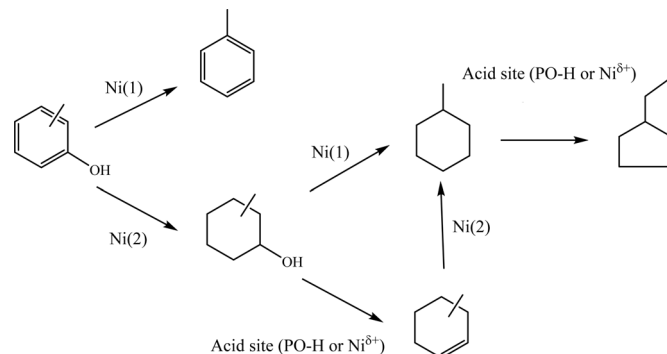
Entry	Reaction temperature (°C)	H_2 pressure (MPa)	τ (g h mol^{-1})	Conversion (%)	Selectivity (mol%)						1-MCHe/MCHes
					Tol	3-MCHnone	3-MCHols	MCHes	MCH	ECP	
1	250	3.2	90.0	8.9	5.2	13.8	8.4	38.5	33.8	0.3	69
2	300	3.2	15.0	10.0	13.9	11.4	4.3	26.8	42.9	0.7	67
3	340	3.2	5.0	12.8	20.7	5.3	0.0	22.0	51.2	0.8	64
4	340	2.4	6.0	10.8	24.5	22.8	0.0	8.5	43.6	0.6	64
5	340	1.6	7.0	10.5	26.2	25.4	0.0	7.8	40.2	0.4	64

point of view, as k_{HYD} was more affected by pressure than k_{DDO}, toluene (DDO product) must be less favored than deoxygenated products (methylcyclohexenes and methylcyclohexane) obtained by the HYD route, as shown in Table 5. In addition, the selectivity to methylcyclohexane increased only slightly compared to methyl-cyclohexenes when the partial pressure of H_2 increased. This result may be attributed to the competition between hydrogenolysis and dehydration reactions, the former could be less favored by H_2 than the dehydration of alcohols.
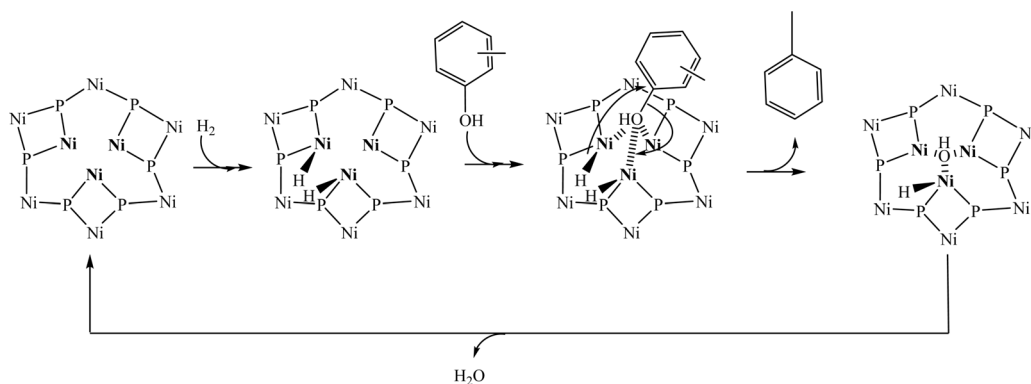
A crystal of Ni_2P presents an orthorhombic structure constituted by two kinds of P atoms, P(1) and P(2), and two types of Ni, Ni(1) and Ni(2) [29,39,68,69]. Ni(1) atoms exhibit a near tetrahedral structure whereas Ni(2) atoms have a square pyramidal structure. Along the (0001) direction of Ni_2P bulk, two stacked structures, Ni_3P and Ni_3P_2 are alternatively placed. The former is composed by Ni(2) and P(1) and the latter by Ni(1) and P(2). Based on DFT studies, it was proposed that the termination of the crystal with Ni_3P_2 was more stable than the Ni_3P [68,70]. However, both surface terminations were observed by photoemission electron microscopy [71].
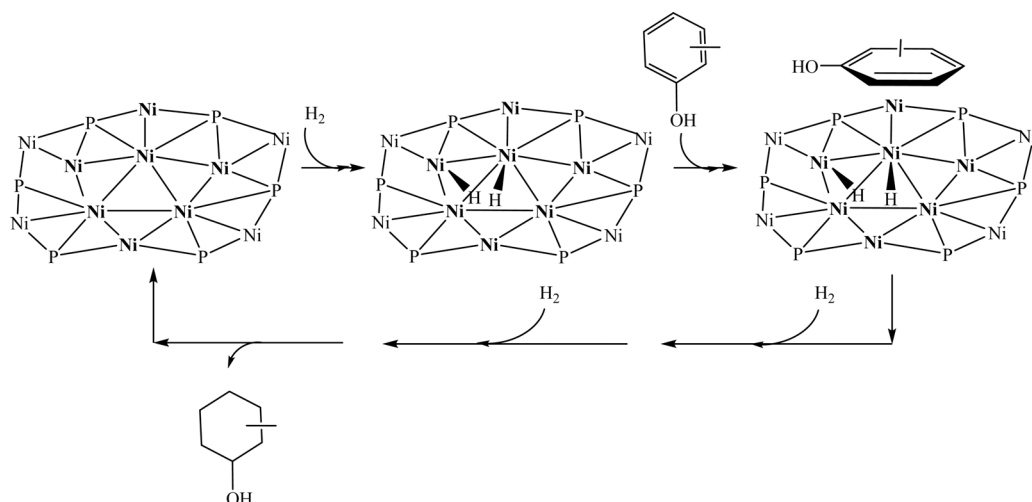
For the HDS of 4,6-dimethyldibenzothiophene, it was proposed that Ni(1), which has a lower coordination number, was likely to be involved in the DDS route leading to dimethylbiphenyl, while Ni(2) could be responsible of the HYD route yielding methylcyclo-hexyltoluenes [72,73]. These results indicate that the Ni_3P surface, composed by Ni(2) atoms, could exhibit high hydrogenation properties whereas the Ni_3P_2, composed by Ni(1), allows the direct C-S bond scission. Similarly to HDS, Feitosa et al. proposed that DDO active sites for the HDO of guaiacol involves Ni(1) [74]. According to theoretical calculations [39,68], it was suggested the existence of an hollow site on the Ni_3P_2 surface involving three Ni(1) neighbor atoms. Such site was proposed as an active site for the DDO route of guaiacol since it allowed a strong adsorption of the OH group by the oxygen atom [39]. Similarly, it was proposed that Ni(1) could act as an adsorption site for 2-methyltetrahydropyran through its oxygen atom [75].

In turn, based on our experimental results, several types of active sites present on the nickel phosphide phase can be considered to explain the reactivity of cresols (Scheme 2). It can then be suggested that the C—O bond scission leading to toluene from the

Scheme 2. Proposals of the different active sites likely to occur transformation of cresols over Ni_2P phase.

cresol isomers and to methylcyclohexane from methylcyclohex-anols took place on the same kind of active site, which could involve the participation of three neighboring Ni(1) on the Ni_3P_2 surface, as already proposed for other oxygenated compounds [39,74,75]. After the dissociation of H_2 on Ni(1) atoms, the adsorption of cresol through its oxygen atom could take place on a schematic hollow site presented in Scheme 3. The C—O bond scission can occur by a nucle-ophilic attack of a hydride species on the carbon bearing the OH group, which results in the formation of toluene. The same type of mechanism can be assumed to explain the formation of methylcy-clohexane from methylcyclohexanols. As already discussed above, the rates of these reactions are estimated by the values of k_{DDO} and k_1 for the formation of toluene and methylcyclohexane, respectively. The fact that these values were the lowest when o-cresol was used as reactant can be explained by a steric effect due to the presence of methyl group on the α-carbon (Table 4). In addition, as m-cresol and the alcohols obtained by hydrogenation of this cresol isomer exhibits the highest reactivity, the presence of the methyl group on the carbon in β position seems to better activate the C—O bond scission compared to the other isomers, which may be related to electronic effects.

Scheme 3. Proposals for the formation of toluene from cresol on a schematic hollow site composed by three neiboring Ni(1) on the Ni_3P_2 termination (adapted from [69]).

Scheme 4. Proposal mechanism for the formation of methylcyclohexanol from cresol on a schematic Ni_3P termination (adapted from [69]).

Concerning the HYD route, as proposed recently [72,73], we suggest that the initial steps of this deoxygenation route could be performed on Ni_3P termination, involving Ni(2) species, as indicated in Scheme 4. Differently to the DDO route, a flat adsorption through the aromatic ring could be considered in this case. Such adsorption mode may explain why the position of the methyl group has little effect on the k_{HYD} values, as shown in Table 4. Indeed, theoretical calculation would be needed to prove this assumption. However, this proposition related to the experimental data seem reasonable. The presence of PO—H sites as Brønsted acid sites on the phosphide phase can explain the presence of products obtained by dehydration (methylcyclohexenes) and isomerization (mixture of alkenes in thermodynamic equilibrium and ethylcyclopentane) as indicated in Scheme 3. Nevertheless, the participation of the Lewis acidity, due to $Ni^{\delta+}$, cannot be ruled out. To confirm such proposals concerning the adsorption modes and reaction mechanisms further investigations are required, especially by using DFT methods.

4. Conclusion

The present study investigated the HDO of cresols isomers over Ni_2P/SiO_2 catalyst, which involved two parallel deoxygenation routes. Different reactions such as hydrogenolysis, hydrogenation, dehydration and isomerization took place on this catalyst leading to several products. The main pathway (so-called HYD) led to oxygenated (ketones and alcohols) and deoxygenated products (cycloalkenes and cycloalkane), whereas the DDO route yielded only toluene by hydrogenolysis of the C—O bond. The use of a relative high pressure of hydrogen (3.2 MPa) allowed to ensure a remarkable stability of the nickel phosphide phase. An effect of the position of the methyl group was highlighted, depending on the pathway considered. The reactivity of cresols followed: m-cresol > p-cresol > o-cresol, the DDO route being more affected by the position of the methyl group than the HYD route. This result suggests that active sites involved in both deoxygenation routes could be different. The effect of temperature and hydrogen pressure was also dependent on the deoxygenation route: temperature favored more the DDO route whereas an increase of the hydrogen pressure was more beneficial for the HYD route. Nevertheless, it is important to underline that an increase of both experimental parameters allowed a higher deoxygenation degree of m-cresol (close to 100%), in spite of low conversion rates (lower than 20%).

Based on these experimental results, several kinds of active sites and adsorption modes were proposed to explain the formation of the products observed experimentally. The Ni(1) sites present

on the Ni_3P_2 termination seem to be associated to hydrogenolysis reactions which take place in the transformation of cresols into toluene and methylcyclohexanols into methylcyclohexane. These reactions probably need an activation of the C—O bond through the adsorption by the oxygen atom. On the opposite, Ni(2) sites, presents on the Ni_3P termination, are likely to be active for hydrogenation of aromatic ring, probably suggesting a flat adsorption of cresols. In addition, Brønsted acid sites (probably PO—H groups) as well as Lewis acid sites ($Ni^{\delta+}$ species) were involved in dehydration and isomerization reactions.

Acknowledgments

Appendix A. Supplementary data

Supplementary data associated with this article can be found, in the online version, at http://dx.doi.org/10.1016/j.apcatb.2016.12.051.

References

[1] G.W. Huber, A. Corma, Angew. Chem. Int. Ed. 46 (2007) 7184–7201.
[2] D.M. Alonso, J.Q. Bond, J.A. Dumesic, Green Chem. 12 (2010) 1493–1513.
[3] J. Zakzeski, P.C.A. Bruijnincx, A.L. Jongerius, B.M. Weckhuysen, Chem. Rev. 110 (2010) 3552–3599.
[4] S.K. Maity, Renew. Sustain. Energy Rev. 43 (2015) 1427–1445.
[5] G.W. Huber, S. Iborra, A. Corma, Chem. Rev. 106 (2006) 4044–4098.
[6] C. Li, X. Zhao, A. Wang, G.W. Huber, T. Zhang, Chem. Rev. 115 (2015) 11559–11624.
[7] E. Furimsky, Catal. Today 217 (2013) 13–56.
[8] N. Arun, R.V. Sharma, A.K. Dalai, Renew. Sustain. Energy Rev. 48 (2015) 240–255.
[9] M. Patel, A. Kumar, Renew. Sustain. Energy Rev. 58 (2016) 1293–1307.
[10] H. Wang, J. Male, Y. Wang, ACS Catal. 3 (2013) 1047–1070.
[11] S. De, B. Saha, R. Luque, Bioresour. Technol. 178 (2015) 108–118.
[12] E. Furimsky, Appl. Catal. Gen. 199 (2000) 147–190.
[13] M. Saidi, F. Samimi, D. Karimipourfard, T. Nimmanwudipong, B.C. Gates, M.R. Rahimpour, Energy Environ. Sci. 7 (2014) 103–129.
[14] D.A. Ruddy, J.A. Schaidle, J.R.F. Iii, J. Wang, L. Moens, J.E. Hensley, Green Chem. 16 (2014) 454–490.
[15] O. Şenol, T.-R. Viljava, A. Krause, Appl. Catal. Gen. 326 (2007) 236–244.

[16] E.-M. Ryymin, M.L. Honkela, T.-R. Viljava, A.O.I. Krause, Appl. Catal. Gen. 358 (2009) 42–48.
[17] S. Brillouet, E. Baltag, S. Brunet, F. Richard, Appl. Catal. B Environ. 148–149 (2014) 201–211.
[18] C. Zhao, Y. Kou, A.A. Lemonidou, X. Li, J.A. Lercher, Angew. Chem. 121 (2009) 4047–4050.
[19] P.M. Mortensen, J.-D. Grunwaldt, P.A. Jensen, A.D. Jensen, ACS Catal. 3 (2013) 1774–1785.
[20] P.M. de Souza, L. Nie, L.E.P. Borges, F.B. Noronha, D.E. Resasco, Catal. Lett. 144 (2014) 2005–2011.
[21] P.M. de Souza, R.C. Rabelo-Neto, L.E.P. Borges, G. Jacobs, B.H. Davis, T. Sooknoi, D.E. Resasco, F.B. Noronha, ACS Catal. 5 (2015) 1318–1329.
[22] M.B. Griffin, G.A. Ferguson, D.A. Ruddy, M.J. Biddy, G.T. Beckham, J.A. Schaidle, ACS Catal. (2016) 2715–2727.
[23] M.V. Bykova, D.Y. Ermakov, V.V. Kaichev, O.A. Bulavchenko, A.A. Saraev, M.Y. Lebedev, V.A. Yakovlev, Appl. Catal. B Environ. 113–114 (2012) 296–307.
[24] I. Rossetti, C. Biffi, C.L. Bianchi, V. Nichele, M. Signoretto, F. Menegazzo, E. Finocchio, G. Ramis, A. Di Michele, Appl. Catal. B Environ. 117–118 (2012) 384–396.
[25] L. Nie, P.M. de Souza, F.B. Noronha, W. An, T. Sooknoi, D.E. Resasco, J. Mol. Catal. Chem. 388–389 (2014) 47–55.
[26] C.A. Teles, R.C. Rabelo-Neto, J.R. de Lima, L.V. Mattos, D.E. Resasco, F.B. Noronha, Catal. Lett. 146 (2016) 1848–1857.
[27] S.T. Oyama, T. Gott, H. Zhao, Y.-K. Lee, Catal. Today 143 (2009) 94–107.
[28] A.-M. Alexander, J.S.J. Hargreaves, Chem. Soc. Rev. 39 (2010) 4388–4401.
[29] R. Prins, M.E. Bussell, Catal. Lett. 142 (2012) 1413–1436.
[30] S. Carenco, D. Portehault, C. Boissière, N. Mézailles, C. Sanchez, Chem. Rev. 113 (2013) 7981–8065.
[31] Y. Yang, J. Chen, H. Shi, Energy Fuels 27 (2013) 3400–3409.
[32] J. Chen, H. Shi, L. Li, K. Li, Appl. Catal. B Environ. 144 (2014) 870–884.
[33] Z. Zhang, M. Tang, J. Chen, Appl. Surf. Sci. 360 (2016) 353–364.
[34] Y. Li, X. Yang, L. Zhu, H. Zhang, B. Chen, RSC Adv. 5 (2015) 80388–80396.
[35] K. Yan, Y. Li, X. Zhang, X. Yang, N. Zhang, J. Zheng, B. Chen, K.J. Smith, Int. J. Hydrogen Energy 40 (2015) 16137–16146.
[36] A. Berenguer, T.M. Sankaranarayanan, G. Gómez, I. Moreno, J.M. Coronado, P. Pizarro, D.P. Serrano, Green Chem. 18 (2016) 1938–1951.
[37] H. Zhao, D. Li, P. Bui, S. Oyama, Appl. Catal. Gen. 391 (2011) 305–310.
[38] S.-K. Wu, P.-C. Lai, Y.-C. Lin, H.-P. Wan, H.-T. Lee, Y.-H. Chang, ACS Sustain. Chem. Eng. 1 (2013) 349–358.
[39] J.-S. Moon, E.-G. Kim, Y.-K. Lee, J. Catal. 311 (2014) 144–152.
[40] S.-K. Wu, P.-C. Lai, Y.-C. Lin, Catal. Lett. 144 (2014) 878–889.
[41] M.B. Griffin, F.G. Baddour, S.E. Habas, D.A. Ruddy, J.A. Schaidle, Top. Catal. 59 (2016) 124–137.
[42] V.M.L. Whiffen, K.J. Smith, Top. Catal. 55 (2012) 981–990.
[43] W. Wang, K. Zhang, H. Liu, Z. Qiao, Y. Yang, K. Ren, Catal. Commun. 41 (2013) 41–46.
[44] A. Infantes-Molina, E. Gralberg, J.A. Cecilia, E. Finocchio, E. Rodríguez-Castellón, Catal. Sci. Technol. 5 (2015) 3403–3415.
[45] K. Li, R. Wang, J. Chen, Energy Fuels 25 (2011) 854–863.

[46] J. Cecilia, A. Infantes-Molina, E. Rodríguez-Castellón, A. Jiménez-López, S. Oyama, Appl. Catal. B Environ. 136 (2013) 140–149.
[47] C. Kordulis, K. Bourikas, M. Gousi, E. Kordouli, A. Lycourghiotis, Appl. Catal. B Environ. 181 (2016) 156–196.
[48] E. Laurent, B. Delmon, Ind. Eng. Chem. Res. 32 (1993) 2516–2524.
[49] O.İ. Şenol, E.-M. Ryymin, T.-R. Viljava, A.O.I. Krause, J. Mol. Catal. Chem. 277 (2007) 107–112.
[50] C. Bouvier, Y. Romero, F. Richard, S. Brunet, Green Chem. 13 (2011) 2441–2451.
[51] V.O.O. Gonçalves, S. Brunet, F. Richard, Catal. Lett. 146 (2016) 1562–1573.
[52] L. Nie, D.E. Resasco, J. Catal. 317 (2014) 22–29.
[53] V.M.L. Whiffen, K.J. Smith, S.K. Straus, Appl. Catal. Gen. 419–420 (2012) 111–125.
[54] S. Oyama, X. Wang, F. Requejo, T. Sato, Y. Yoshimura, J. Catal. 209 (2002) 1–5.
[55] G.F. Froment, K.B. Bischoff, J.D. Wilde, Chemical Reactor Analysis and Design, 3 edition, Wiley, Hoboken, NJ, 2010.
[56] P.M. Mortensen, D. Gardini, H.W.P. de Carvalho, C.D. Damsgaard, J.-D. Grunwaldt, P.A. Jensen, J.B. Wagner, A.D. Jensen, Catal. Sci. Technol. 4 (2014) 3672–3686.
[57] Q. Guan, X. Cheng, R. Li, W. Li, J. Catal. 299 (2013) 1–9.
[58] S.T. Oyama, X. Wang, Y.-K. Lee, K. Bando, F.G. Requejo, J. Catal. 210 (2002) 207–217.
[59] G. Leofanti, M. Padovan, G. Tozzola, B. Venturelli, Catal. Today 41 (1998) 207–219.
[60] Y.-K. Lee, S.T. Oyama, J. Catal. 239 (2006) 376–389.
[61] S.T. Oyama, X. Wang, Y.-K. Lee, W.-J. Chun, J. Catal. 221 (2004) 263–273.
[62] J.A. Cecilia, A. Infantes-Molina, E. Rodríguez-Castellón, A. Jiménez-López, J. Phys. Chem. C 113 (2009) 17032–17044.
[63] A. Iino, A. Cho, A. Takagaki, R. Kikuchi, S.T. Oyama, J. Catal. 311 (2014) 17–27.
[64] D. Li, P. Bui, H.Y. Zhao, S.T. Oyama, T. Dou, Z.H. Shen, J. Catal. 290 (2012) 1–12.
[65] N. Koike, S. Hosokai, A. Takagaki, S. Nishimura, R. Kikuchi, K. Ebitani, Y. Suzuki, S.T. Oyama, J. Catal. 333 (2016) 115–126.
[66] M. Peereboom, B. Van de Graaf, J.M.A. Baas, Recl. Trav. Chim. Pays-Bas 101 (1982) 336–338.
[67] F. Massoth, P. Politzer, M. Concha, J. Murray, J. Jakowski, J. Simons, J. Phys. Chem. B 110 (2006) 14283–14291.
[68] A.E. Nelson, M. Sun, A.S.M. Junaid, J. Catal. 241 (2006) 180–188.
[69] Q. Yuan, H. Ariga, K. Asakura, Top. Catal. 58 (2015) 194–200.
[70] P. Liu, J.A. Rodriguez, T. Asakura, J. Gomes, K. Nakamura, J. Phys. Chem. B 109 (2005) 4575–4583.
[71] S. Suzuki, G.M. Moula, T. Miyamoto, Y. Nakagawa, K. Kinosthita, K. Asakura, S.T. Oyama, S. Otani, J. Nanosci. Nanotechnol. 9 (2009) 195–201.
[72] S.T. Oyama, Y.-K. Lee, J. Catal. 258 (2008) 393–400.
[73] H. Zhao, S.T. Oyama, H.-J. Freund, R. Włodarczyk, M. Sierka, Appl. Catal. B Environ. 164 (2015) 204–216.
[74] L.F. Feitosa, G. Berhault, D. Laurenti, T.E. Davies, V. Teixeira da Silva, J. Catal. 340 (2016) 154–165.
[75] P.P. Bui, S.T. Oyama, A. Takagaki, B.P. Carrow, K. Nozaki, ACS Catal. 6 (2016) 4549–4558.